Proceedings of the 9th International Conference on Physical Modelling in Coastal Engineering (Coastlab24)

Delft, Netherlands, May 13-16, 2024

Conference Paper, DOI: 10.59490/coastlab.2024.685

APPLICABILITY OF REFLECTION SEPARATION ALGORITHMS TO NONLINEAR IRREGULAR WAVES OVER SLOPING FORESHORES

LYKKE ANDERSEN, T.[1], ELDRUP, M. R. [2]

1 Dept. of the Built Environment, Aalborg University, Denmark, tla@build.aau.dk

2 Dept. of the Built Environment, Aalborg University, Denmark, mrel@build.aau.dk

ABSTRACT

In hydraulic model tests, it is common practice to relate the response of the tested structure to the incident wave parameters at the toe. Estimation of the incident wave parameters at the toe is thus an essential part of the analysis of hydraulic model testing. In many cases, the design conditions at the toe are given by waves that are highly nonlinear or even depth limited. Modelling such conditions requires reproducing the prototype foreshore slope in the model. The present paper provide guidelines on the accuracy of a nonlinear reflection separation algorithm when applied to nonlinear waves over sloping foreshores. A simple methodology has been established to estimate the expected errors on the incident wave parameters.

KEYWORDS: Reflection separation, incident waves, nonlinear waves, foreshore, shoaling.

1 INTRODUCTION

When a coastal structure is exposed to waves, a part of the incident energy is reflected back to the sea. In hydraulic model tests, this reflection poses several difficulties. Firstly, the reflected waves will be re-reflected at the wavemaker and thus a compensation of the steering signal is needed to keep control of the incident waves. This active absorption compensation is used to generate a wave opposite to the re-reflected so they cancel each other, cf. Lykke Andersen et al. (2016). Secondly, if the reflection coefficient is large, standing waves are formed, and they produce unwanted cross-modes more easily than progressive waves. Thirdly, as only the sum of the incident and reflected surface elevation can be measured, it is not straightforward to determine the incident wave parameters. The present paper deals with the third effect, which is essential for relating the response of the tested structure to the incident wave parameters at the toe. For coastal structures, the design conditions at the toe are in many cases given by depth-limited waves or at least nonlinear waves. In both cases the wave transformation on the foreshore depends significantly on the foreshore slope and thus it must be reproduced in the model. Most methods for separation of incident and reflected waves are not valid for sloping foreshores, leading to unknown uncertainties for the incident wave parameters at the toe. The aim of the present paper is to quantify this uncertainty.

Lykke Andersen and Eldrup (2021) divided the methods for the estimation of the incident waves into three classes of methods. The first method is to measure without the model in place. The second class of methods is to measure several co-located quantities in a single point, cf. Guza and Bowen (1976) and Kubota et al. (1990). The third class of methods is based on using a spatial array of usually surface elevation gauges. The advantages and disadvantages of the three methods were discussed in Lykke Andersen and Eldrup (2021). The present paper deals with the third class of methods. Several researchers have proposed such a method where most are based on linear wave theory, cf. Goda and Suzuki (1976), Mansard and Funke (1980) and Zelt and Skjelbreia (1992). These linear methods have been used in many labs and provide reliable results as long as the waves are linear and on horizontal foreshore. By inclusion of linear shoaling these methods may be extended to sloping foreshores as described by Baldock and Simmonds (1999).

Extensions to nonlinear waves over horizontal foreshore have been provided by Figueres and Medina (2004) and Eldrup and Lykke Andersen (2019). In the present paper, the Eldrup and Lykke Andersen (2019) method will be considered as it showed large improvements compared to both the linear methods and the nonlinear method of Figueres and Medina (2004). The irregular wave separation method by Eldrup and Lykke Andersen (2019) is building on top of knowledge from mildly nonlinear regular waves by Lin and Huang (2004) method and the extension to highly nonlinear regular waves by Lykke Andersen et al. (2017). An intermediate step to bichromatic waves was presented in Lykke Andersen et al. (2019).

For regular waves, Lykke Andersen and Eldrup (2021) provided the necessary extensions to sloping foreshores by including the nonlinear shoaling model of Eldrup and Lykke Andersen (2020). Thus, the next step needed is an extension of the Eldrup and Lykke Andersen (2019) method to sloping foreshores for irregular waves. This is expected to provide similar

improvement for irregular waves as Lykke Andersen and Eldrup (2021) did for regular waves. However, such extension would require a detailed understanding of the shoaling of irregular nonlinear waves and a description hereof in the frequency domain. Such a description is not presently available and several approximations would thus be needed.

The aim of the present paper is to provide guidelines on the accuracy of reflection separation algorithms valid for horizontal foreshores when applied to nonlinear irregular waves over sloping foreshores. The guidelines will present examples of the error in the estimated incident wave parameters depending on the wave nonlinearity and the foreshore slope.

2 APPLIED REFLECTION SEPARATION ALGORITHM

The applied method is the state-of-the-art frequency domain method by Eldrup and Lykke Andersen (2019) for irregular waves. Their method is building on top of the knowledge for regular and bichromatic waves. The spectrum is divided into a subharmonic, primary and several superharmonics bands and a they provided a mathematical model for each band. For the sub and superharmonic bands both free and bound waves are present in the mathematical model and they may be separated due to the difference in their celerity. This was initially demonstrated by Lin and Huang (2004) for regular waves. In all bands, amplitude dispersion is described by a simplified methodology (β_I and β_R factors). By utilizing a narrow band assumption for the primary spectrum, the phase velocity of the various components in the various bands could be described. The results of Eldrup and Lykke Andersen (2019) indicated that normal spectra were also well described with only minor errors on the assumed celerities. For the present paper, the method is used with an alternative criteria for whether an accurate solution with all terms may be obtained or not. The mathematical model of the waves used by Eldrup and Lykke Andersen (2019) is separated into various regions of the spectrum, each with its own mathematical model. In the frequency domain, it can for the primary region be written as:

$$\widehat{\eta}(\omega, x_m) = C_I^{(1)} X_I^{(1)} + C_R^{(1)} X_R^{(1)} + \Omega_m \tag{1}$$

$$X_I^{(1)} = a_I(\omega) \exp\left[-i\left(\beta_I\, k(\omega,h)\, x_1 + \varphi_I(\omega)\right)\right]$$

$$X_R^{(1)} = a_R(\omega) \exp\left[i\left(\beta_R\, k(\omega,h)\, x_1 + \varphi_R(\omega)\right)\right]$$

$$C_I^{(1)} = \exp(-i\beta_I\, k(\omega,h)\Delta x_m)$$

$$C_R^{(1)} = \exp(i\beta_R\, k(\omega,h)\Delta x_m)$$

For the subharmonic region:

$$\widehat{\eta}(\omega, x_m) = C_{I,B}^{(-1)} X_{I,B}^{(-1)} + C_{R,B}^{(-1)} X_{R,B}^{(-1)} + C_{I,F}^{(-1)} X_{I,F}^{(-1)} + C_{R,F}^{(-1)} X_{R,F}^{(-1)} + \Omega_m \tag{2}$$

$$X_{I,B}^{(-1)} = a_{I,B}(\omega) \exp\left[-i\left(\omega\beta_I / c_g(f_p,h) x_1 + \varphi_{I,B}(\omega)\right)\right]$$

$$X_{R,B}^{(-1)} = a_{R,B}(\omega) \exp\left[i\left(\omega\beta_R / c_g(f_p,h) x_1 + \varphi_{R,B}(\omega)\right)\right]$$

$$X_{I,F}^{(-1)} = a_{I,F}(\omega) \exp\left[-i\left(k(\omega,h) x_1 + \varphi_{I,F}(\omega)\right)\right]$$

$$X_{R,F}^{(-1)} = a_{R,F}(\omega) \exp\left[i\left(k(\omega,h) x_1 + \varphi_{R,F}(\omega)\right)\right]$$

$$C_{I,B}^{(-1)} = \exp(-i\omega\beta_I / c_g(f_p,h)\Delta x_m)$$

$$C_{R,B}^{(-1)} = \exp(i\omega\beta_R / c_g(f_p,h)\Delta x_m)$$

$$C_{I,F}^{(-1)} = \exp(-ik(\omega,h)\Delta x_m)$$

$$C_{R,F}^{(-1)} = \exp(ik(\omega,h)\Delta x_m)$$

For the superharmonic region:

$$\widehat{\eta}(\omega, x_m) = C_{I,B}^{(n)} X_{I,B}^{(n)} + C_{R,B}^{(n)} X_{R,B}^{(n)} + C_{I,F}^{(n)} X_{I,F}^{(n)} + C_{R,F}^{(n)} X_{R,F}^{(n)} + \Omega_m \tag{3}$$

$$X_{I,B}^{(n)} = a_{I,B}(\omega) \exp\left[-i\left(n\beta_I\, k(\omega/n,h) x_1 + \varphi_{I,B}(\omega)\right)\right]$$

$$X_{R,B}^{(n)} = a_{R,B}(\omega) \exp\left[i\left(n\beta_R\, k(\omega/n,h) x_1 + \varphi_{R,B}(\omega)\right)\right]$$

$$X_{I,F}^{(n)} = a_{I,F}(\omega) \exp\left[-i\left(k(\omega,h) x_1 + \varphi_{I,F}(\omega)\right)\right]$$

$$X_{R,F}^{(n)} = a_{R,F}(\omega) \exp\left[i\left(k(\omega,h) x_1 + \varphi_{R,F}(\omega)\right)\right]$$

$$C_{I,B}^{(n)} = \exp(-in\beta_I\, k(\omega/n,h)\Delta x_m)$$

$$C_{R,B}^{(n)} = \exp(in\beta_R\, k(\omega/n,h)\Delta x_m)$$
$$C_{I,F}^{(n)} = \exp(-ik(\omega,h)\Delta x_m)$$
$$C_{R,F}^{(n)} = \exp(ik(\omega,h)\Delta x_m)$$

Refer to Eldrup and Lykke Andersen (2019) for a detailed explanation of the symbols in above equations. Lykke Andersen et al. (2017) and Eldrup and Lykke Andersen (2019) describe that the reliability of the separation into free and bound components in the sub and superharmonic regions depends on the ratio of the bound and free wave celerities. This give different formulae for the sub and superharmonic bands. For the superharmonic frequencies Eq. 4 applies:

$$\alpha_I = \frac{c_{bound}}{c_{free}} = \frac{k(\omega,h)}{n\beta_I\, k(\omega/n,h)} \tag{4}$$

When $\alpha_I < 1.05$ the separation in bound and free waves should not be performed as the mathematical problem is close to being singular, while for $1.05 < \alpha_I < 1.15$, the reliability of the separation should be based on additional checks. An additional condition was added by Lykke Andersen and Eldrup (2021) to consider the phase difference over the length of the array:

$$\beta_I = [k(\omega,h) - n\beta_I\, k(\omega/n,h)]\Delta x \tag{5}$$

where Δx is the length of the wave gauge array. Lykke Andersen and Eldrup (2021) suggested that for $\beta_I < 0.03\pi$ the separation in bound and free incident wave components should also not be performed. For $0.03\pi < \beta_I < 0.08\pi$ the reliability of the separation should be based on additional checks. Equations 4 and 5 are presented for the incident waves, but identical checks are performed to check if reflected wave separation in bound and free components is reliable.

Recently, De Ridder et al. (2023) suggested instead using the condition number (C) of the phase matrix to quantify whether the separation is reliable or not. The condition number describes if the mathematical problem is well-conditioned (low condition number) or ill-conditioned (high condition number). It describes the sensitivity of the solution to small variations in the inputs. De Ridder et al. (2023) studied the influence of the limit of the condition number to reduce the number of unknowns similar to Lykke Andersen et al. (2017), i.e. when not to separate in bound and free components. Based hereon they suggest the limit of the condition number to be 20.

As part of the present paper, it was studied if the condition number could replace the conditions used previously as given in Eqs. 4 and 5. Many model tests were analysed, and based heron it was found that in shallow water, a blown-up solution may also occur for condition numbers between 5 and 20. This is because the condition number does not consider that for smaller values of α, relatively small errors on the estimated celerities may have a large influence on the solution. A condition number limit of 5 would significantly limit the application of the method. Thus, in the present paper the condition number is used in combination with the criteria in Eq. 4. Additional verify criteria are used to check for a blown-up solution and thus the condition number and α values do not need to be conservatively selected and thus values given in Table 1 are used. If any of the reject criteria are fulfilled, the mathematical model must be reduced to not separate in bound and free components at that frequency. If any of the verify criteria are fulfilled, the solution is checked against additional criteria to identify possible blown-up solutions. If the condition number criteria suggests that the mathematical problem should be reduced, it is firstly reduced for the reflected waves, and if the condition number criteria still suggests it should be reduced it is also reduced for the incident waves.

Shoaling is not considered in the mathematical model as linear shoaling is not valid for the studied conditions and shoaling of nonlinear irregular waves is not yet properly described in the literature. Instead, it is the aim of the present paper to quantify the errors of the method due to the lack of shoaling in the mathematical model.

Table 1. Criteria for selecting if the mathematical model may include all terms.

	Condition number		Celerity ratio
Reject solution	$C \geq 100$	or	$\alpha \leq 1.05$
Verify solution	$5 < C < 100$	or	$1.05 < \alpha < 1.15$
Accept solution	$C < 5$	and	$\alpha \geq 1.15$

3 NUMERICAL MODEL DATA

The data used to evaluate the performance of the Eldrup and Lykke Andersen (2019) reflection separation method on sloping foreshores was generated by the numerical model MIKE 3 Wave FM, cf. DHI (2024). The model is a Reynolds Averaged Navier-Stokes model (RANS) where the vertical coordinate is transformed into sigma coordinates. Using sigma

coordinates leads to a computationally efficient model as the air phase is not modelled. This is because of fewer grid cells may be used in a single phase model and also that larger time steps may often be used as it is not restricted by the Currant number in the air phase. The turbulence model used is a k-ε model and no bottom friction was used. The temporal discretization is given by a Currant number of 0.8 and 10 vertical layers is used in the model. For the horizontal spatial discretization, 200 grid elements per wavelength calculated by the linear dispersion relation with T_p and the smallest depth in the model.

The bathymetry used is shown in Figure 1. The waves were generated at a depth of h_{deep} = 1.5 m and shoaled over different foreshore slopes to a depth of $h_{shallow}$ = 0.5 m. The large depth in the wave generation zone was needed as waves were generated by linear theory. The seabed slopes tested were β = cot(angle) = 250, 100, 50, 30 and 20. This range covers the typical range used in hydraulic model testing. No structure is included in the numerical model and thus the reflection coefficient is low due to the highly effective passive absorber. Thus, the only expected reflection in the model is the reflection from the foreshore which must be expected to be small unless the foreshore is very steep. Even if this is not the typical scenario for application of reflection analysis it was chosen to assess the uncertainty of the estimated incident waves for a case where the target incident waves are known. For cases with reflections similar errors must be expected for the incident waves.

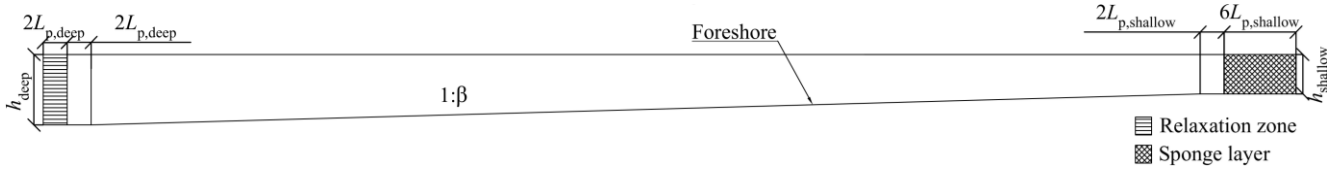

Figure 1. Numerical model layout.

Five sea states were used as shown in Table 2. Sea state 1 and 2 represent typical design sea states modelled in a small scale hydraulic laboratory at a scale of approximately 1:50. Sea state 1 would correspond to a site dominated by sea waves and sea state 2 a site dominated by swell waves. Sea states 3 to 5 are conditions with very low steepness and represent low steepness swell conditions modelled in a scale of approximately 1:20. A JONSWAP spectrum with a peak enhancement factor of γ = 3.3 is used for all sea states. Spectra for swell seas will typically have a larger peak enhancement factor, but this is not taken into account in the present test cases. This is expected to provide safe application ranges of the reflection separation method which is based on narrow-band approximation for the primary spectrum.

In the shallow end of the model the highest waves are in several cases around the breaking limit, but the waves can be characterized mainly as non-breaking on the foreshore. Sea states 2 to 5 are highly nonlinear waves at the shallow end of the model with significant superharmonic energy being present. Sea states 3 to 5 are not typical extreme conditions but may be very relevant for operational conditions. An example of such operation criteria would be overtopping on breakwaters.

Table 2. The sea states generated.

	$H_{m0,deep}$ [m]	T_p [s]	$h_{shallow}/L_{0p}$ [-]	s_{0p} [-]
Sea state 1	0.100	2.0	0.080	0.0160
Sea state 2	0.100	3.0	0.036	0.0071
Sea state 3	0.100	4.0	0.020	0.0040
Sea state 4	0.100	5.0	0.013	0.0026
Sea state 5	0.150	5.0	0.013	0.0038

Fig. 2 shows the shoaling of the waves in the numerical model for Sea state 4 and foreshore slopes 1:250 and 1:20. Included is also curves for linear shoaling and nonlinear shoaling from the deep section. These shoaling curves are based on regular waves with a period equal to the peak wave period. The nonlinear shoaling curve is based on conservation of the energy flux in nonlinear regular waves, cf. Rienecker and Fenton (1981). The linear shoaling shows the best estimate for the shoaling for the selected wave heights. Figure 3 shows the development of the spectrum for the same two cases and shows that the shoaling is completely different on the steep and the gentle foreshore. For the gentle slope, the shoaling significantly increases the bound subharmonic and superharmonic energy. For the steep slope, the subharmonic is hardly visible and the growth in the superharmonic peak is also much less than for the gentle slope. Similar was found by Eldrup and Lykke Andersen (2020) for shoaling of the superharmonics in regular waves, but the effect is even more pronounced for the irregular waves. This strong influence of the foreshore slope on the shoaling means that an accurate engineering shoaling model is difficult to develop. Thus, it will be difficult to include nonlinear shoaling in Eqs. 1-3 in an accurate manner.

For each numerical test case, 100 data sets along the foreshore slope were generated for reflection analysis. For each data set, wave gauge array with 7 gauges were extracted from the numerical model. Gauge spacings were selected as x_{12}/L_p = 0.05, x_{13}/L_p = 0.12, x_{14}/L_p = 0.21, x_{15}/L_p = 0.27, x_{16}/L_p = 0.31 and x_{17}/L_p = 0.45. Finally, two additional output gauges are used to extract the waves in the middle of the array x_{18}/L_p = 0.225 and outside of the array x_{19}/L_p = 0.85. WG9 is used to check the accuracy of waves extrapolated to the toe, if the last gauge in the wave gauge array is placed $0.4L_p$ from the toe. This was chosen to study the recommandation by Klopman and Van der Meer (1999) based on evanescent waves near the structure.

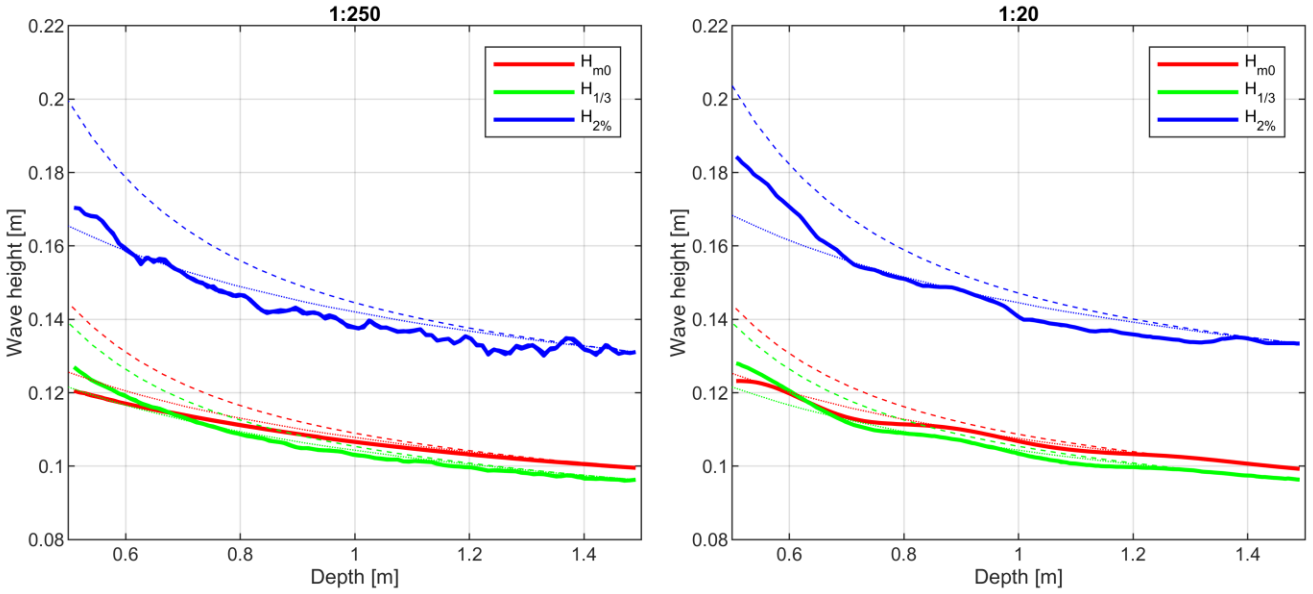

Figure 2. Development of the wave height along the foreshore for Sea state 4 and foreshore slopes 1:250 and 1:20. Solid lines are numerical data, dotted curves linear shoaling and dashed curves nonlinear shoaling.

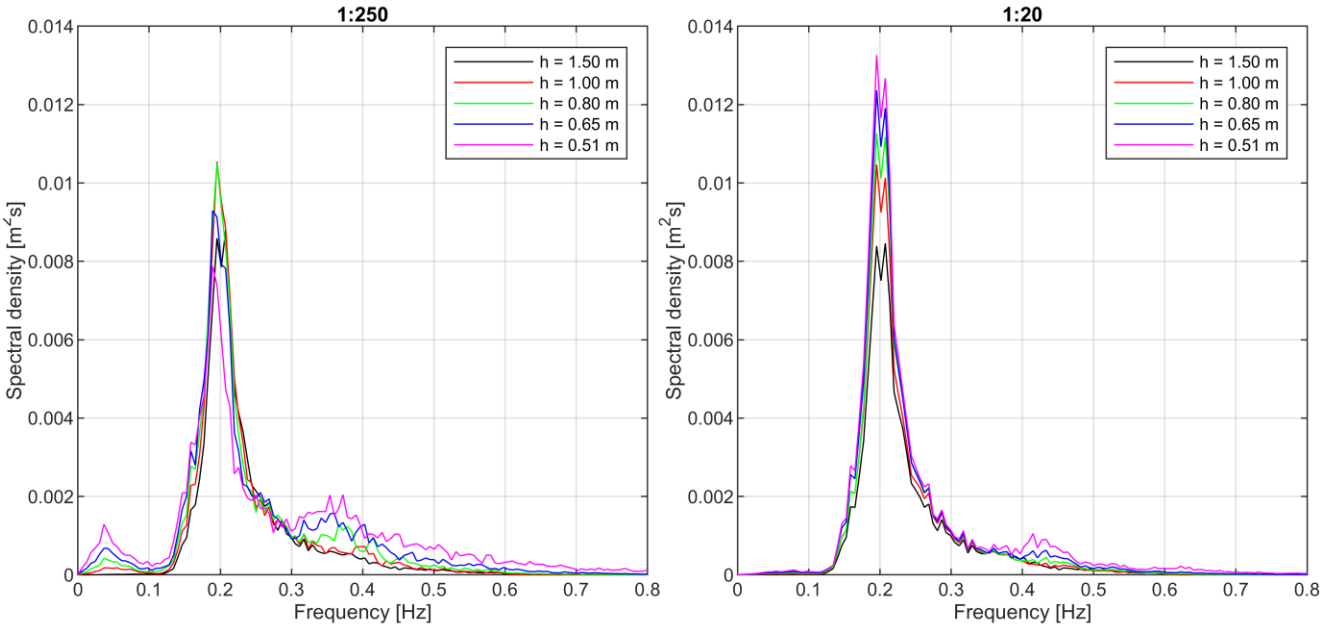

Figure 3. Development of the spectrum along the foreshore for Sea state 4 and foreshore slopes 1:250 and 1:20.

4 RESULTS

After applying the Eldrup and Lykke Andersen (2019) method, a mathematical description exists for the sea state, cf. Eqs. 1-3. Thus, it is possible to evaluate the incident and reflected wave train in any given x-coordinate. In the present paper, predictions are provided in four *x*-coordinates, corresponding to start of the array (WG1), middle of the array (WG8), end of the array (WG7) and extrapolated to the toe of a structure following Klopman and Van der Meer (1999) criteria (WG9).

Figure 4 shows an example of the predicted and target time series in these four locations for a foreshore slope 1:250 and Sea state 4. The time window shown is at the instance of the highest wave crest in the time series. The wave gauge array considered is with the last gauge 0.4 L_p from the termination of the foreshore slope, cf. Fig. 1. The α value for the second-order superharmonic peak is 1.098 for the incident waves and 1.046 for the reflected waves. Thus, the reflected waves are not separated into bound and free components at the second-order peak, cf. Table 1. Under that constraint the condition number in the second-order superharmonic region is 5-10, meaning that incident waves can be separated into bound and free components, but results will be verified, cf. Table 1. The incident wave train is well predicted in the middle of the array, while

the predictions are slightly worse at the start and end of the array. When the waves are extrapolated outside of the array (WG9), the error increases dramatically in this case. The variance of the error signal relative to the variance of the target signal is shown in the legend. This ratio is given for the entire time series and not the shown time window. The errors occur because the numerical data does not correspond perfectly to the mathematical model in Eqs. 1-3 with the assumed simplified amplitude dispersion and the missing shoaling model. Thus, free waves are found even if mainly bound energy is present at the higher harmonic frequencies. These errors are amplified when the wave train is extrapolated outside of the array due to the difference in celerity for the free and bound waves. It also appears that errors below $5 \cdot 10^{-3,}$ even for the highest waves, only lead to minor differences on the time series.

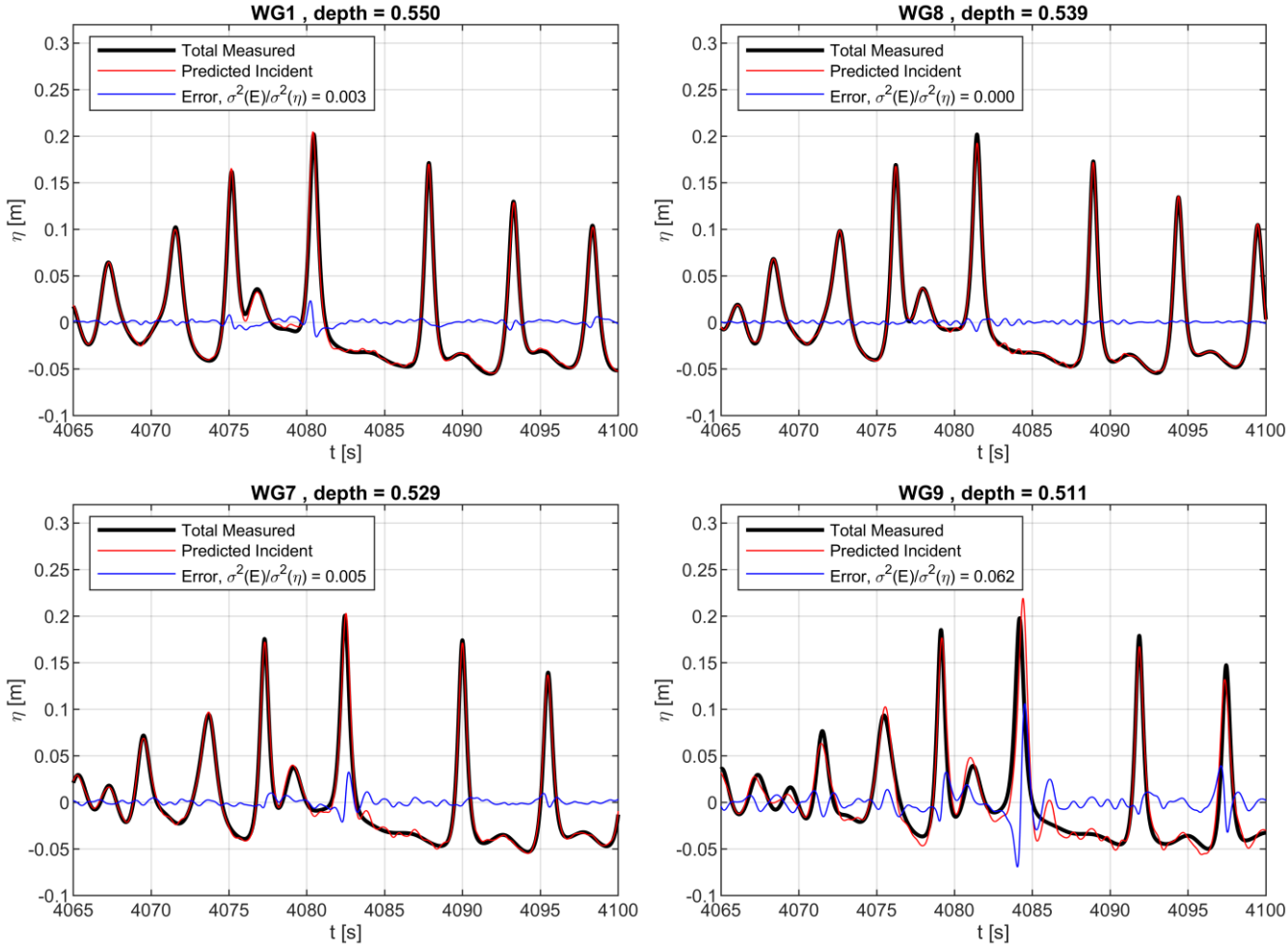

Figure 4. Predicted incident waves compared with the target for Sea state 4 on the 1:250 slope.

Fig. 5 shows the same as Fig. 4, but for a foreshore slope of 1:20 instead. Despite not including shoaling in the mathematical model, the error is even for this highly nonlinear case small for WG1, WG8 and WG7. However, the height of the highest wave is overpredicted at the start of the array (WG1) and underpredicted in the end of the array (WG7). Very large errors occur on the predicted waves outside of the array (WG9). A combination of free and bound waves might partly describe the nonlinear shoaling inside the array. Thus, the found distribution of free and bound wave amplitudes does not describe the real distribution of the energy, but they also compensate for the errors in the applied mathematical model. In the present case neglecting shoaling introduce large errors as the amplitude increase and the phase velocity decrease over the length of the array. When these components are extrapolated outside of the array then large errors might occur as demonstrated by this example. Care should thus be taken when waves are extrapolated outside of the array. As the errors are significant even for mildly sloping foreshores, it is not recommended to extrapolate the results so far outside of the array. Thus, Klopman and Van der Meer (1999) recommendations should be revisited as the evanescent modes close to structures might lead to less error in the reflection analysis than the errors from extrapolating the waves 40% of the peak wavelength. This also shows inclusion of an engineering shoaling model in the reflection separation method is needed in order to reduce errors when extrapolating waves outside of the array. The analysis presented in Figs. 4 and 5 has been performed in every of the test cases and for the 100 arrays along the foreshore. This gave the results in Fig. 6 with respect to the variance of the error signal relative to the variance of the target signal. The conclusion is that the error increases with both foreshore slope and wave nonlinearity. The

prediction error in WG8 (middle of the array) is acceptable even for steep foreshores and nonlinear waves. The prediction error in each end of the array (WG1 and WG7) are up to approximately one order of magnitude higher. This applies even for the very mildly sloping foreshore of 1:250, but as shown by Fig. 4 the consequence for the gentle 1:250 slope is small as error is always below $5 \cdot 10^{-3}$. Moreover, it appears that the prediction error in WG9 (extrapolated $0.4L_p$ from the last gauge) is for mildly sloping foreshores typically one order of magnitude higher than in the ends of the array. This increases to almost two orders of magnitudes higher at the steep foreshores and highly nonlinear waves. The consequence of these errors on the predicted wave heights are shown in Figs. 7-9. Also shown are shoaling coefficients from the middle of the array to the ends and to WG9. These shoaling coefficients are for regular waves with a period equal to T_p. Curves are shown for linear shoaling and nonlinear shoaling, cf. Rienecker and Fenton (1981). The shoaling curves demonstrate that the linear shoaling curve gives an upper limit on the errors for the spectral wave height and the nonlinear shoaling curve for the time domain wave heights. Thus, the estimated wave height errors might be explained by not including shoaling in the mathematical model.

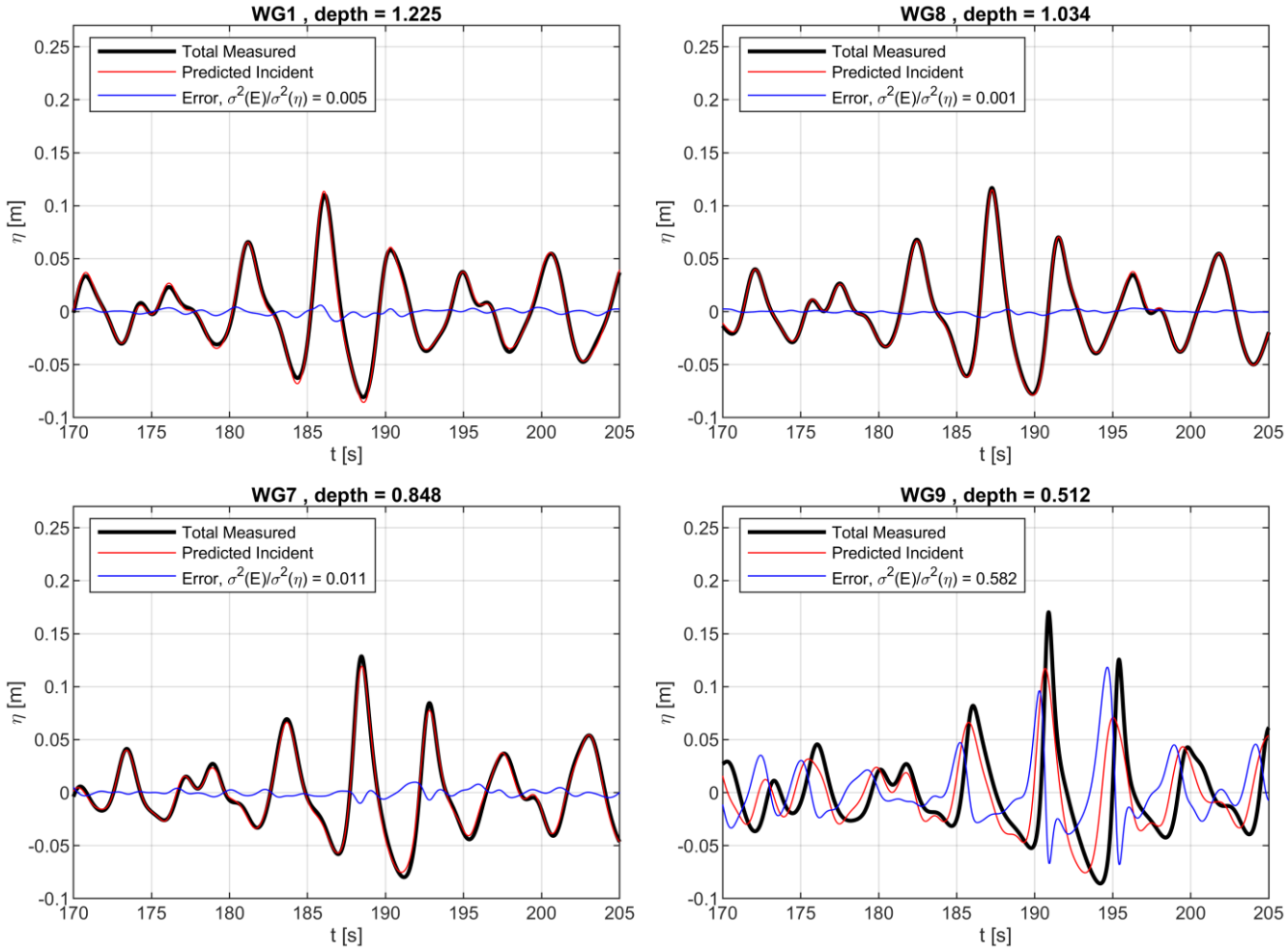

Figure 5. Predicted incident waves compared with the target for Sea state 4 on the 1:20 slope.

5 GUIDELINES FOR APPLICABILITY

The expected error on the wave parameters obtained by Eldrup and Lykke Andersen (2019) for sloping foreshores has been studied. For all sea states and all wave parameters the error is small and acceptable in the middle of the wave gauge array. The error increases towards the ends of the array and even further when extrapolated outside of the array. For the spectral wave height (H_{m0}) the expected error may be found by the linear shoaling coefficient from the middle of the array to the point in question. For the $H_{1/3}$ and $H_{2\%}$ wave heights, the expected error may be found by nonlinear shoaling from the middle of the array to the point in question.

In order to extent the applicability of Eldrup and Lykke Andersen (2019) to steep foreshores, it is necessary to include shoaling in the mathematical model in Eqs. 1-3. This would require a model for the shoaling of the waves in the various bands, i.e. changes in amplitude and celerity of the various components. If such shoaling model is available, it can be included in the mathematical model similarly to what has been done for regular waves by Lykke Andersen and Eldrup (2021).

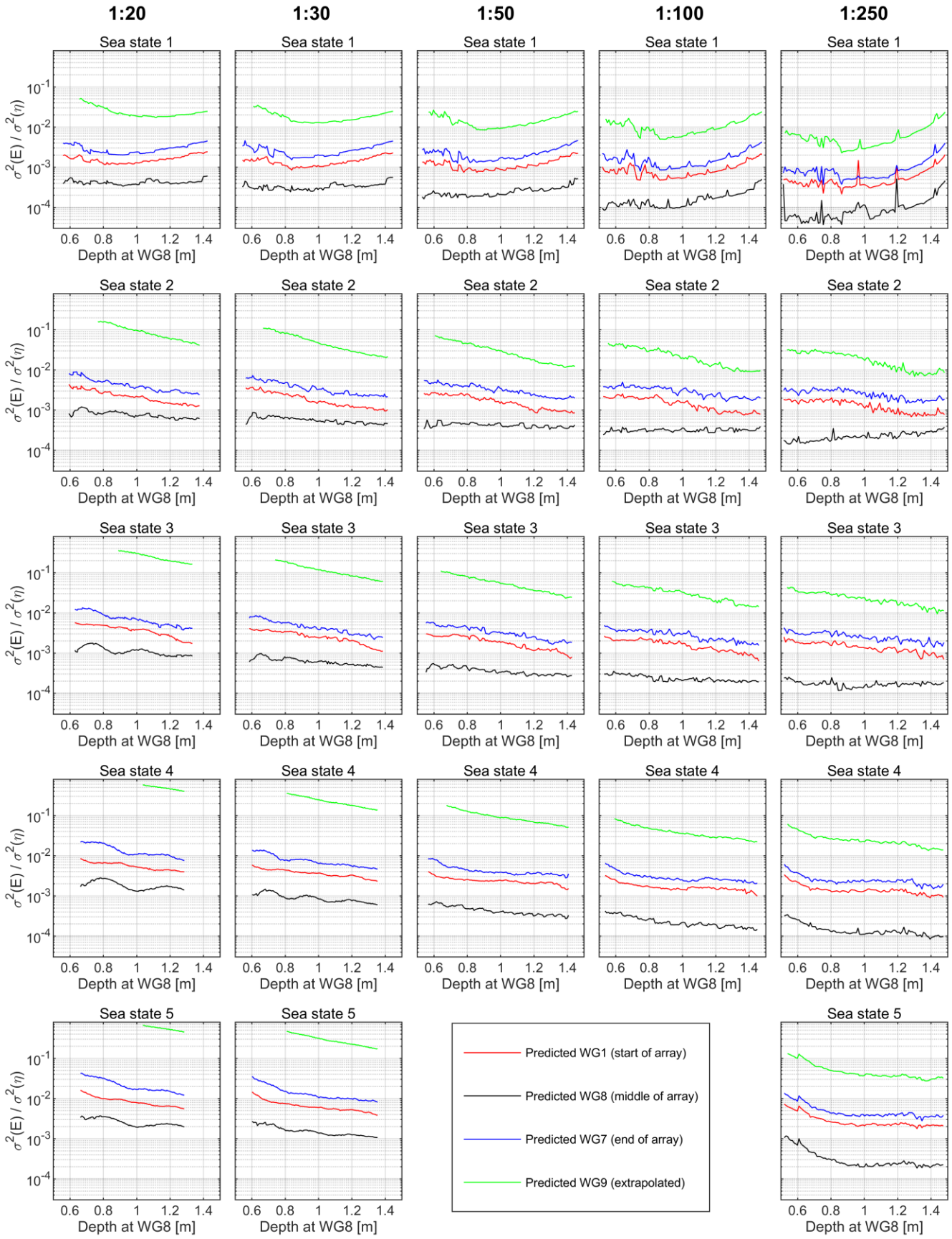

Figure 6. Variance of the error time series compared to the variance of the target time series. Error time series is calculated from the predicted and target time series, i.e. $\eta_{error}(t) = \eta_{predicted}(t) - \eta_{target}(t)$.

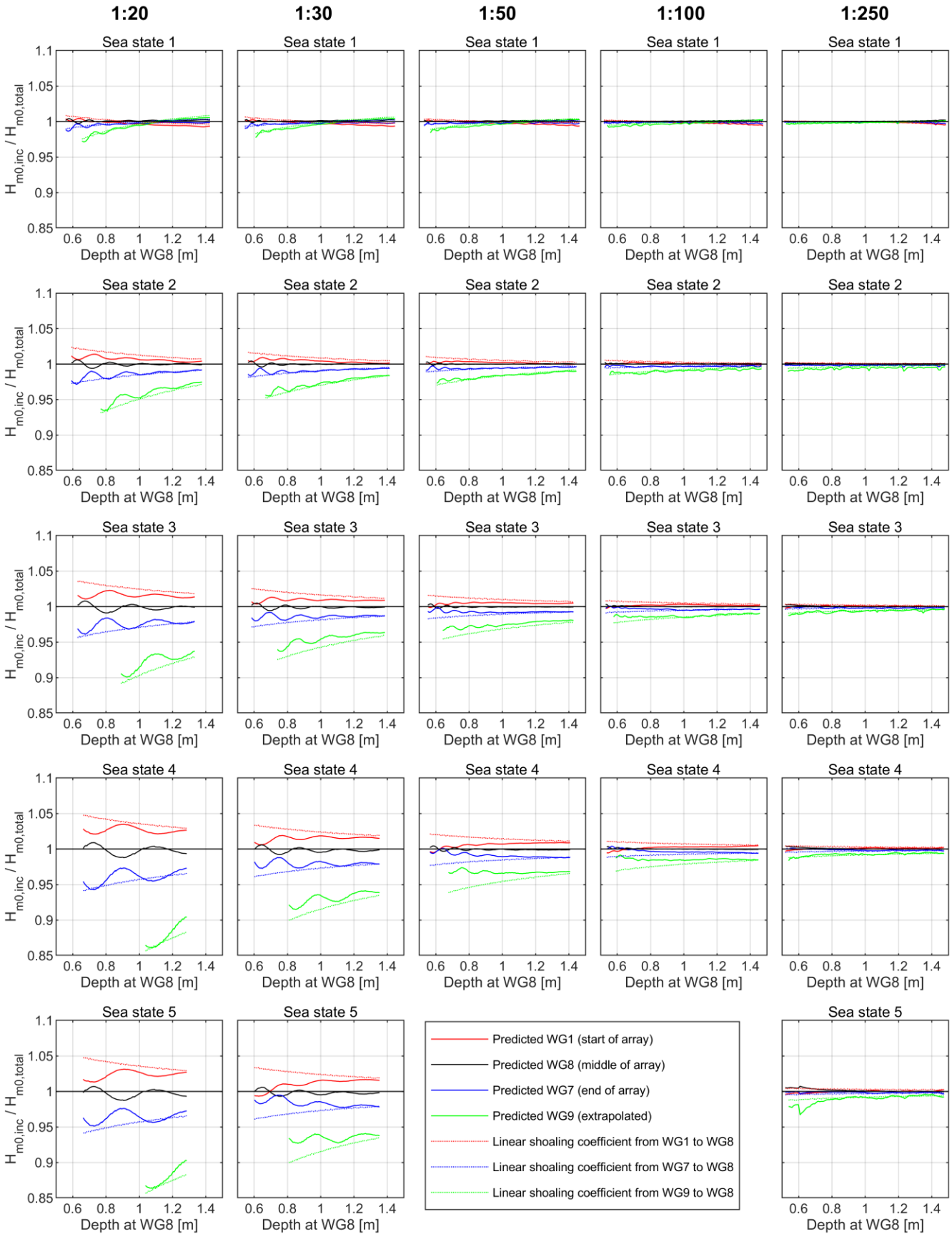

Figure 7. Ratio of predicted and target spectral wave height for all sea states and foreshore slopes. Shoaling coefficients are calculated using the peak wave period.

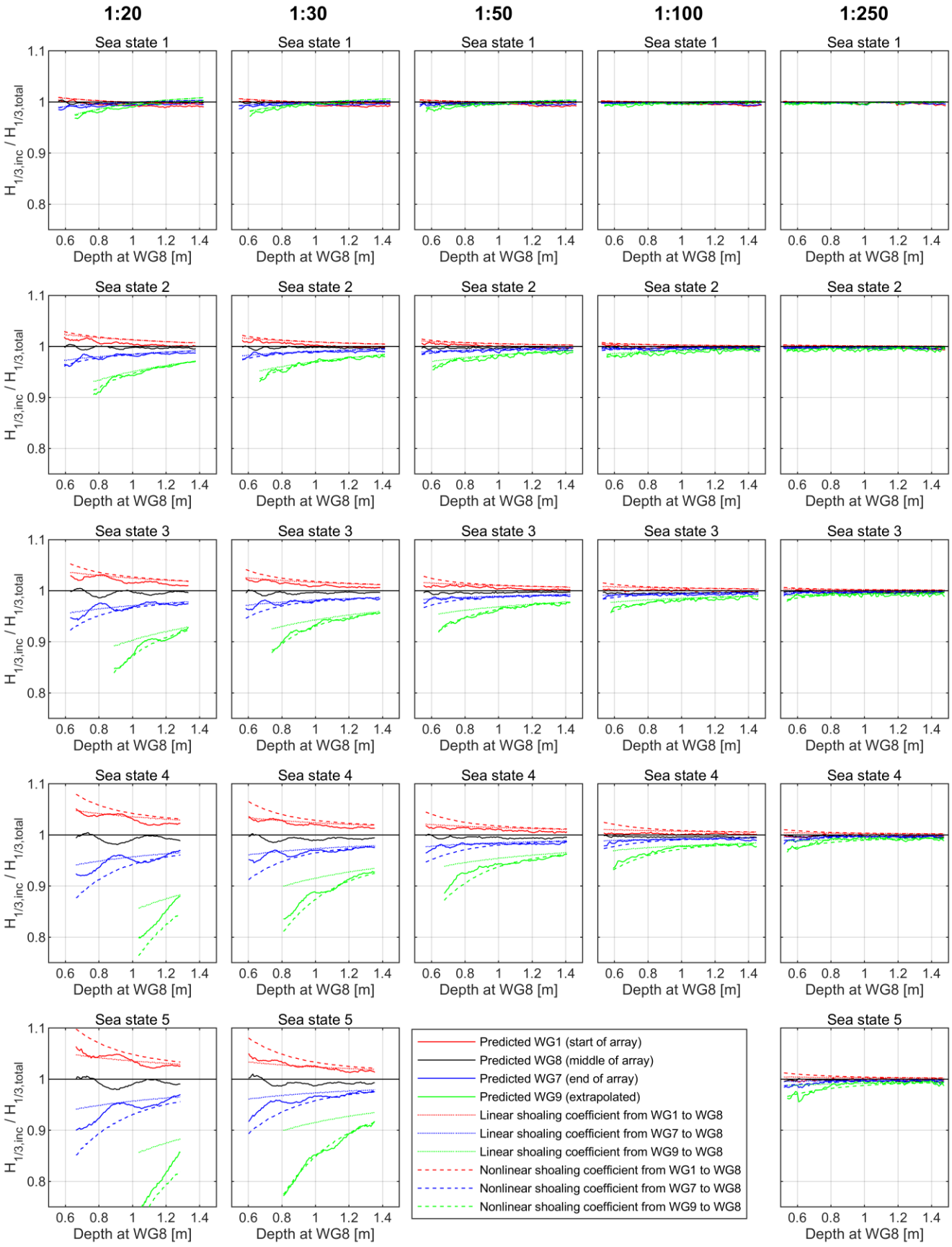

Figure 8. Ratio of predicted and target significant wave height for all sea states and foreshore slopes. Shoaling coefficients are calculated using the peak wave period.

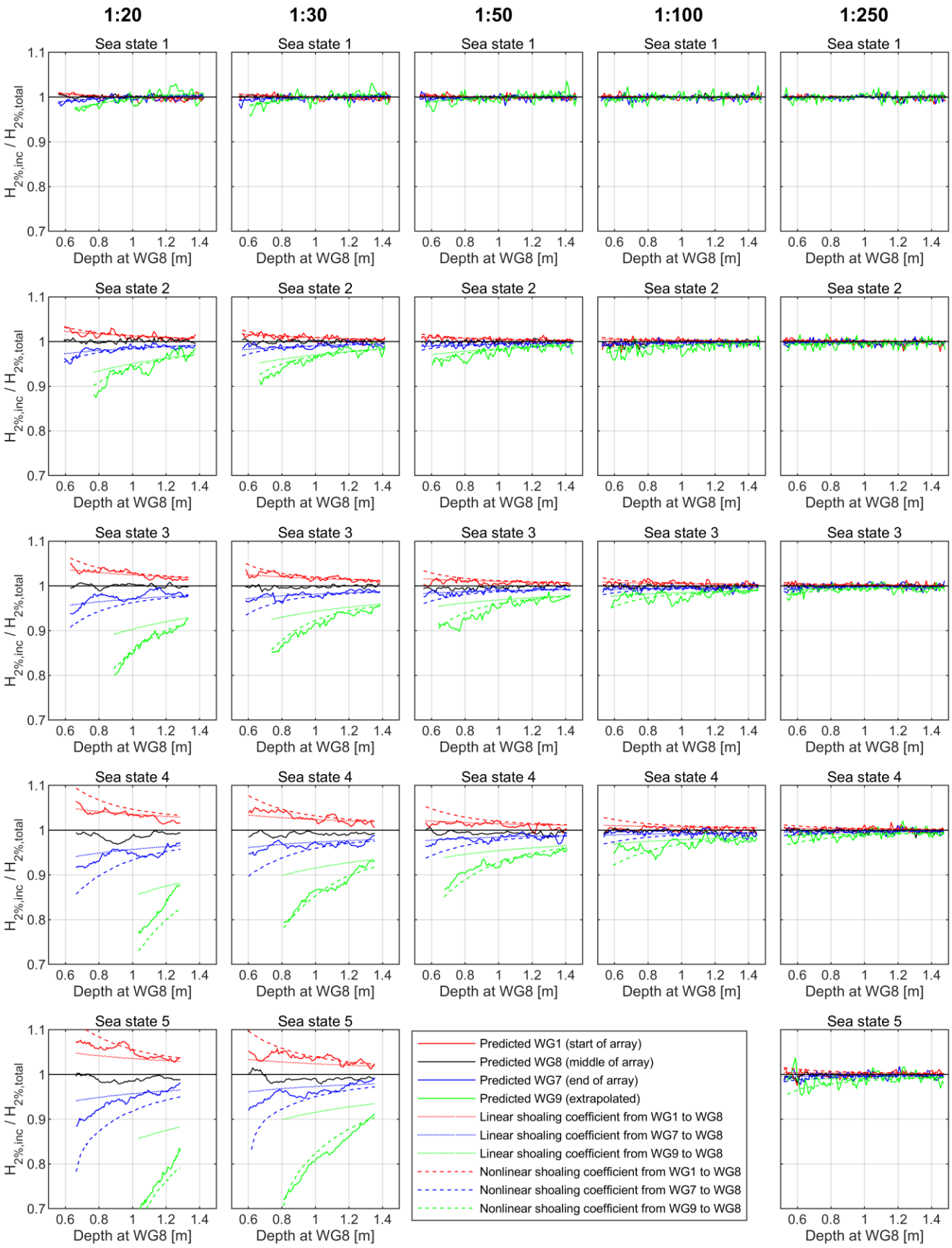

Figure 9. Ratio of predicted and target wave height with 2% exceedance probability for all sea states and foreshore slopes. Shoaling coefficients are calculated using the peak wave period.

6 CONCLUSIONS

In the present paper the applicability of the Eldrup and Lykke Andersen (2019) reflection separation algorithm has been studied for sloping foreshores. The expected errors on surface elevation time series and wave parameters have been quantified for different foreshore slopes and wave nonlinearities. A major conclusion is that in the middle of the wave gauge array, the obtained surface elevation time series and wave parameters have small errors independent of the foreshore slope. The errors in the end of the array are more significant and especially for steep foreshores. Waves extrapolated outside of the array may be associated with very large errors. Thus, the recommendation by Klopman and Van der Meer (1999) of placing the array 40% of the peak wavelength from the toe of the structure should be revisited.

A methodology has been provided to estimate the expected errors on the obtained spectral and time domain wave heights. Future work would be to develop an engineering approximation for shoaling of nonlinear irregular waves and include it in the mathematical model. This is expected to reduce the errors on steep foreshores significantly.

REFERENCES

Baldock, T. E. and Simmonds, D. J. (1999). Separation of incident and reflected waves over sloping bathymetry, *Coastal Engineering*, Vol. 38, pp. 167-176.

De Ridder, M. P., Kramer, J., Den Bieman, J. P. and Wenneker, I. (2023). Validation and practical application of nonlinear wave decomposition methods for irregular waves. Coastal Engineering, Vol. 183, 104311.

DHI (2024). MIKE 3 Wave FM. Hydrodynamic module. Scientific Documentation. DHI, Hørsholm, Denmark.

Eldrup, M. R. and Lykke Andersen, T. (2019). Estimation of Incident and Reflected Wave Trains in Highly Nonlinear Two-Dimensional Irregular Waves. *Journal of Waterway, Port, Coastal, and Ocean Engineering*, Vol. 145, Issue 1 (January 2019).

Eldrup, M. R. and Lykke Andersen, T. (2020). Numerical Study on Regular Wave Shoaling, De-shoaling and Decomposition of Free/Bound Waves on Gentle and Steep Foreshores. *Journal of Marine Science and Engineering*, Vol. 8, Special Issue "Selected Papers from the Future Paths and Needs in Wave Modelling Workshop".

Figueres, M. and Medina, J. R. (2004). Estimating incident and reflected waves using a fully nonlinear wave model. *Proc., 29th Conf. on Coastal Eng.*, Lisbon, Portugal, pp. 594-603.

Goda, Y. and Suzuki, Y. (1976). "Estimation of incident and reflected waves in random wave experiments". *15th International Conference on Coastal Engineering*, Volume 1, Honolulu, pp. 828-845.

Guza and Bowen (1976). Resonant interactions for waves breaking on a beach, *15th International Conference on Coastal Engineering*, Honolulu, Hawaii, United States, pp. 560-579.

Klopman, G. and Van der Meer, J.W. (1999). Random wave measurements in front of reflective structures. Journal of Waterway, Port, Coastal and Ocean Engineering, Vol. 125, Issue 1, pp. 39-45.

Kubota, S., Mizuguchi, M., Takezawa, M., 1990. Reflection from swash zone on natural beaches. *Proc. 22nd Coastal Eng. Conf.*, American Society of Civil Engineers, Reston VA, USA, pp. 570–583.

Lin, C. Y. and Huang, C. J. (2004). Decomposition of incident and reflected higher harmonic waves using four wave gauges. Coastal Engineering, Vol. 51, pp. 395-406.

Lykke Andersen, T., Clavero, M., Frigaard, P., Losada, M. and Puyol, J. I. (2016). A new active absorption system and its performance to linear and non-linear waves. *Coastal Engineering*, Vol.114, August 2016, Pages 47–60.

Lykke Andersen, T., Eldrup, M. R. and Frigaard, P. (2017). Estimation of Incident and Reflected Components in Highly Nonlinear Regular Waves. *Coastal Engineering*, Vol. 119, pp 51-64.

Lykke Andersen, T., Eldrup, M.R., Clavero, M. (2019). Separation of Long-Crested Nonlinear Bichromatic Waves into Incident and Reflected Components. *Journal of Marine Science and Engineering*, Vol. 7, Special Issue "Selected Papers from Coastlab18 Conference"

Lykke Andersen, T. and Eldrup, M. R. (2021). Estimation of incident and reflected components in nonlinear regular waves over sloping foreshores. *Coastal Engineering*, Vol. 169.

Mansard, E. P. D., and Funke E. R. (1980). The measurement of incident and reflected spectra using a least squares method. *17th International Conference on Coastal Engineering*, Volume 1, Sydney, pp. 154–172.

Rienecker, M. M. and Fenton, J. D. (1981). A Fourier approximation method for steady water waves. *J. Fluid Mech.*, Vol. 104, pp. 119-137.

104, 119–137.Zelt, J. A., and Skjelbreia, J. E. (1992). Estimating incident and reflected wave fields using an arbitrary number of wave gauges. *Proceedings of 23rd Conference on Coastal Engineering*, Venice, Italy, pp. 777-789.